SiliconPV 2023, 13th International Conference on Crystalline Silicon Photovoltaics
Module Characterization and Simulation
https://doi.org/10.52825/siliconpv.v1i.944

Published: 27 Feb. 2024

Characterization of Mechanical Strength of Shingle Joints Using Die Shear Tests

Najwa Abdel Latif[1][https://orcid.org/0009-0009-0227-5036], Rachid Lamsairhri[1], and Torsten Rößler[1][https://orcid.org/0000-0002-9297-6136]

[1] Fraunhofer Institute for Solar Energy Systems ISE, Freiburg, Germany

Abstract. For shingle interconnection there is no standard method to characterize the mechanical strength of the shingled joints. Therefore, we studied a die shear test for this purpose. In the first part, a single epoxy-based electrically conductive adhesive (ECA) was used in an industrial shingle stringer to produce shingle strings with different ECA printing widths and curing temperatures. It was observed that the printed ECA area increases at higher curing temperatures due to the increased formation of voids. Shear strength increased with elevating the curing temperature. In the second part of the study, three ECAs with varying glass transition temperature (T_g) were analysed with dynamic mechanical analysis (DMA). The shear strength of the ECAs correlates with the flexibility of the materials. ECA A, with the highest T_g, had the highest shear strength with an average of (25 ± 3) MPa, and ECA B with an average of (24 ± 9) MPa while ECA C had the lowest shear strength with an average of (15 ± 9) MPa. After characterising the shingled full-format PV modules produced using the three ECAs with electroluminescence and *I*–*V* measurements, it was found that the flexibility of the ECAs and the shear strength of the shingled joints had a very small effect on the module performance after thermal cycling 200 and mechanical load 5400 Pa. The ECAs with higher T_g showed more cell fracture but with negligible power loss. The ECA with the lowest T_g led to subtle joint degradation during the tests.

Keywords: Shingling, Electrically Conductive Adhesive ECA, Die Shear Test, Shear Strength, Dynamic Mechanical Analysis DMA, Glass Transition Temperature

1. Introduction

Shingle solar cell interconnection using electrically conductive adhesives (ECAs) have gained significant attention on the market and in the scientific community [1–7]. For strings interconnected with conventional copper ribbons or wires, the peel test is the standard method to characterize the mechanical strength of the interconnection joint [8]. For shingled strings, however, there is no standardized test to determine the joint strength. Thus, using the die shear test is proposed in this work to ascertain the shear strength of shingled joints.

The die shear test, as defined in ref. [9], is used to determine the shear strength of materials. This is done by applying a shear force on a semiconductor die until failure and determining the type of failure that occurs [9]. Subsequently, the die attach medium, and the substrate can be studied [10]. The test has been adopted to the scope of photovoltaic research to study the adhesion of metallization to the solar cell [11]. A lap shear test on shingled solar cells has been applied in ref. [12] to find a dependency of mechanical strength on the type and amount of ECA used. Shear tests for ribbon interconnection have been also studied as an alternative to peel tests [13]. In our study we apply shear force on a shingle joint interconnected

with ECA and study the type of failure that occurs as well as examine the sheared ECA microscopically.

In the first experimental part, the die shear strength is studied depending on the ECA printing width and curing temperature. In the second part, the influence of the mechanical properties of three ECAs with varying glass transition temperature (T_g) on shear strength, full-format shingled PV module performance and reliability tests is studied.

2. Experimental

2.1 Materials

In first part of the study, an ECA based on an epoxy matrix (denoted as “ECA D”) was used. It has 60%-wt. – 80%-wt. of silver combined with (presumably) silver-coated copper particles as fillers. The curing temperature of ECA D was varied to be 110 °C, 150 °C and 190 °C, as well as the screen openings with 0.25 mm width and 0.4 mm width.

In the second part of the study, three chemically similar ECAs from Polytec PT were used. SB1227−20% (ECA A), SB1242 (ECA B) and VP1246-5.3 (ECA C). The latter two are commercially available products. All three ECAs have epoxy as base polymer and a constant 50%-wt. of silver flakes as filler content. The ECA’s formulation was slightly modified by the vendor to yield different T_g, and all of them were cured at 190 °C for three minutes in the industrial stringer.

The solar cells used to fabricate the shingled strings were industrially produced, p-type, Ga-doped, mono-facial PERC in the G1 format (edge length of 158.75 mm). The host wafers were divided using a thermal laser separation process [14] in stripes of the dimension 31.75 × 158.75 mm².

2.2 Methods

2.2.1 Die Shear Tester and Sample Preparation

Pieces with a dimension of 15 mm × 20 mm were cut from the automatically produced shingle strings with direct lasering (Figure 1a). Each piece had exactly one shingle joint (see Figure 3). Those samples were glued onto a 100 mm × 100 mm glass substrate using a tough super glue (Figure 1b). Bending of the upper shingle was limited by placing a supportive solar cell underneath the upper shingle piece (Figure 1c).

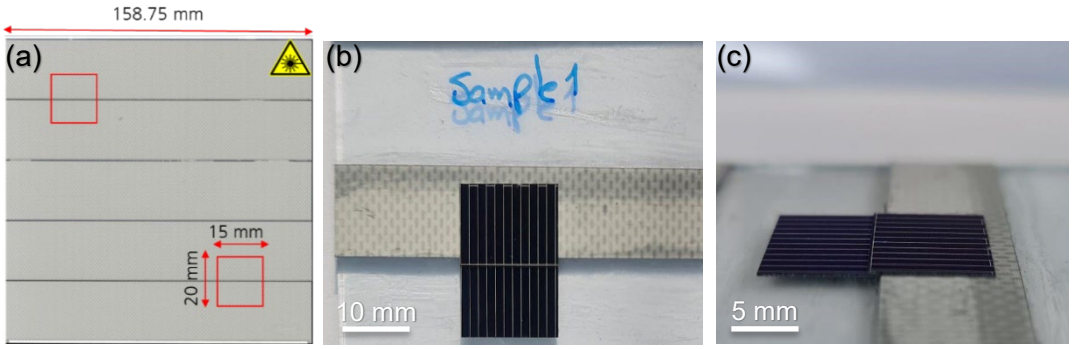

Figure 1. a) Laser cutting of shingle joints for die shear test. b) Top of view of the die shear sample glued on top of a supportive solar cell. c) Side view of the same sample showing the connection between the upper shingle and the supportive solar cells and the lower shingle with the glass

The glass substrate was then placed in a DAGE 1000 multipurpose bond-tester. The shear chisel was 15 mm wide and exerted a force on the upper shingle by movement of the

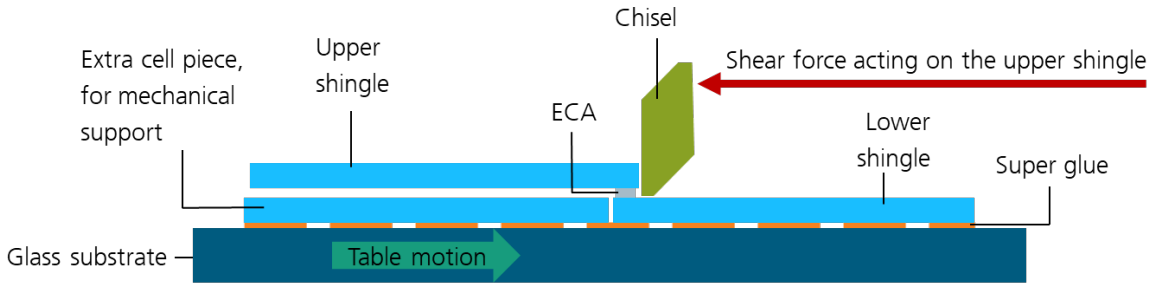

Figure 2. A schematic explaining the die shear test at the DAGE 100 multipurpose bond-tester and the shingle joint fixation on the glass substrate

table. A shear speed of 100 µm/s, a preload of 10 N and a shear height of 40 µm were used. The shear height is the distance of the chisel from the solar cell surface. A schematic of the test is shown in Figure 2. The bond tester records the force applied on the shingle over time and distance of table motion. After fracture took place, the sheared joints were analysed under a microscope (Olympus Digital Microscope DSX 510) with regard to the fracture type [8].

The actual contact area was measured using the remaining of the ECA on the busbar. The shear strength was determined by normalizing the force at fracture to the ECA contact area. Additionally, scanning electron microscopy (SEM) of the voids within ECA B were made. Furthermore, shingle joints were studied using metallography to measure ECA thickness [15].

2.2.2 Dynamic Mechanical Analysis (DMA)

ASTM D4065-95 was used for DMA [16]. According to the norm, the test uses a fixed frequency of oscillation of 1 Hz and a sample heating rate of 2 K/min [17]. The method was employed to ascertain a material's T_g. Tensile test ECA samples were prepared by molding to be rectangular in shape and were cured at 150 °C for 30 minutes in an oven.

2.2.3 Industrial Shingle Stringer and Module Fabrication

A teamtechnik TT1600ECA was used for shingled string production [7]. The stringer applies ECA on the front busbar of the shingles using screen-printing. The shingles have a defined overlap of 1.7 mm. The produced strings were used for full-format module production as well as for die shear characterization.

Shingled strings from ECA A, B and C were laminated into full-size modules using a glass-backsheet configuration. The modules were exposed to thermal cycling between −40 °C and +85 °C for 200 cycles (TC200) and mechanical load (ML5400Pa) reliability tests according to the IEC 61215-2:2016 norm [18]. The modules were characterized using electroluminescence (EL) imaging and current-voltage (*I*–*V*) measurements at initial stage, post-production, after TC200, and after ML5400Pa.

3. Results and Discussion

3.1 Variation of ECA Printing Width and Curing Temperature

From the two different screens and three different curing temperatures studied in this experiment, cross section samples showed very similar average joint thickness of (37 ± 3) µm under the microscope (Figure 3). The results of die shear force and strength with varying screen opening and curing temperature are shown in Figure 4.

Sheared joints of ECA D samples showed that the ECA area increases at higher curing temperatures due to the increased formation of voids. Wider ECA prints led to higher shear forces for all curing temperatures (Figure 4a).

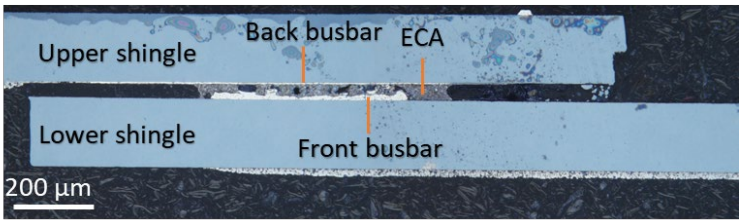

Figure 3. Metallographic cross section of a shingle joint where ECA thickness is measured

Considering shear strength (Figure 4b), a difference between the screens is not obvious. This is expected, as to obtain shear strength, the force is normalized to the actual ECA contact area. It seems that increasing the curing temperature from 110 °C to 150 °C resulted in an increased shear strength (Figure 4b). However, it did not clearly change when going to 190 °C. Curing at 110 °C did not fully establish the mechanical properties and bonding strength of ECA D. However, exceeding 150 °C led to the intended properties. As the die shear test is sensitive to the mechanical properties of the ECA, which is shown in the next section, it can be a useful method to detect too low curing temperatures.

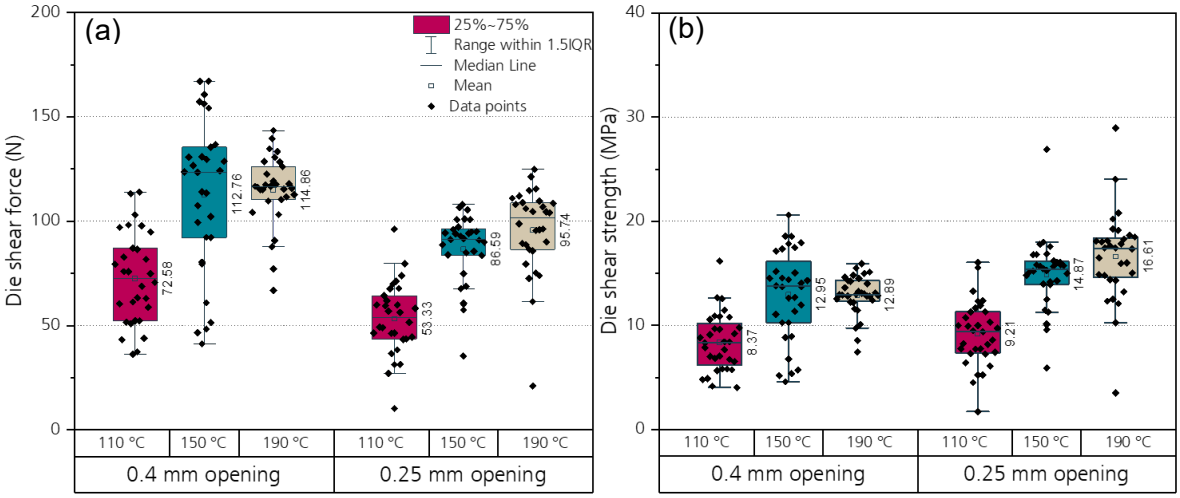

Figure 4. Box-Whisker plots of a) Shear forces and b) shear strength for ECA D for both printing screens and the three different curing temperatures

3.2 Variation of Mechanical Properties of ECA

From the DMA analysis and according to the tan δ, ECA A had the highest glass transition temperature T_g of ~120 °C, as for ECA B it had a T_g of ~90 °C and ECA C had the lowest T_g of ~15 °C (Figure 5a). A PV module's operating temperature range is between −40 °C and +85 °C. As ECA A has a storage modulus E' of 2 GPa to 3 GPa within this temperature range it can be considered stiff. ECA B had an E' in a similar magnitude between −40 °C and +50 °C but started to soften at higher temperatures (Figure 5b). Thus, at the upper operating temperature range of the test procedure, ECA B can be considered an elastomer. In contrast, E' of ECA C was lower than the other two materials over the whole temperature range. In particular, the material had already elastomeric behavior at room temperature.

In the next step of the experiment, the die shear forces, and strengths of shingle strings produced with these three materials were determined. Figure 6a shows a box-whisker plot of

the shear forces and Figure 6b of the shear strengths with the corresponding standard deviations for both. ECA A led to the highest shear force with (249.8 ± 57.3) N ECA B had a shear force of (249.8 ± 57.3) N while ECA C, had a shear force of (174.8 ± 83.3) N. The shear strength, as shown in Figure 6b, mostly followed the same trend. ECA A had (24.9 ± 3.3) MPa, ECA B had (23.6 ± 9.2) MPa, and ECA C had (15.3 ± 8.5) MPa.

The flexibility of the materials at room temperature correlates with the shear strength. ECA A with the lowest flexibility had the highest die shear strength. ECA C with the highest flexibility had the lowest shear strength. ECAs A and B have comparable shear strengths because of the different contact areas.

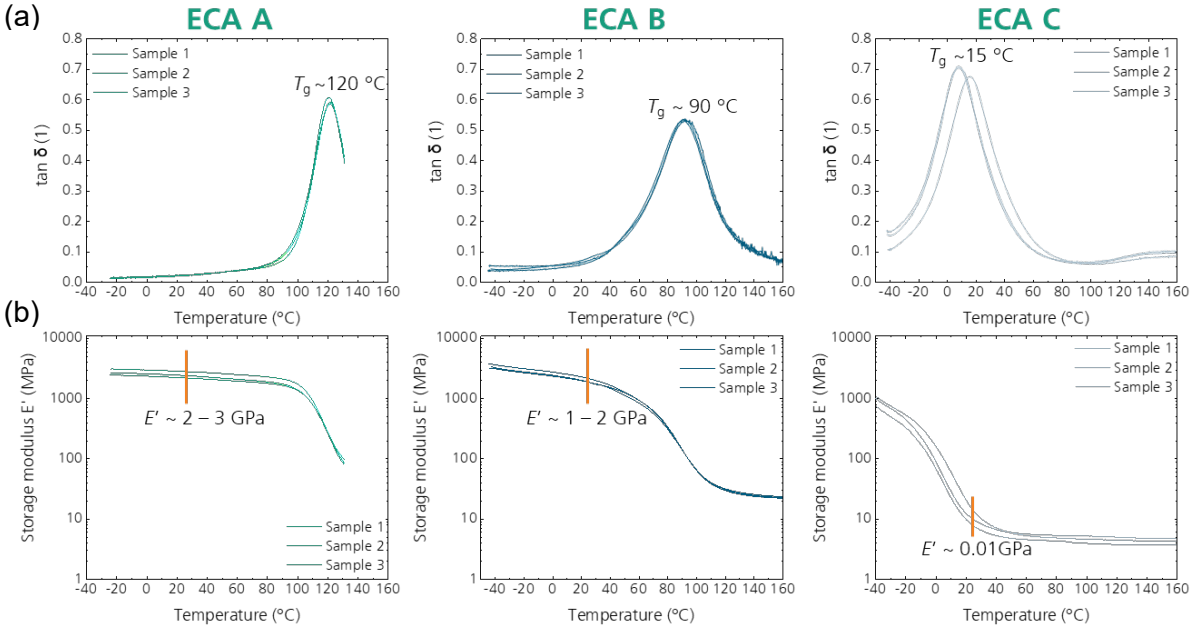

Figure 5. a) The glass transition temperature of the three ECAs according to the peak of tan *δ* indicated on top of each graph. b) Storage modulus of the 3 ECAs at room temperature.

The die shear test tends to have a high tendency for outliers, regardless of the number of samples sheared. In Figure 6 all shear values higher or lower than 2.5 × standard deviation of all data points were discarded. To identify the reason behind the high tendency of outliers, digital and scanning electron microscopy studies were carried out.

About 50 % of the samples sheared from ECA A had substrate fracture (Figure 7a). This indicates that the ECA strength can exceed the fracture strength of the wafer as well as

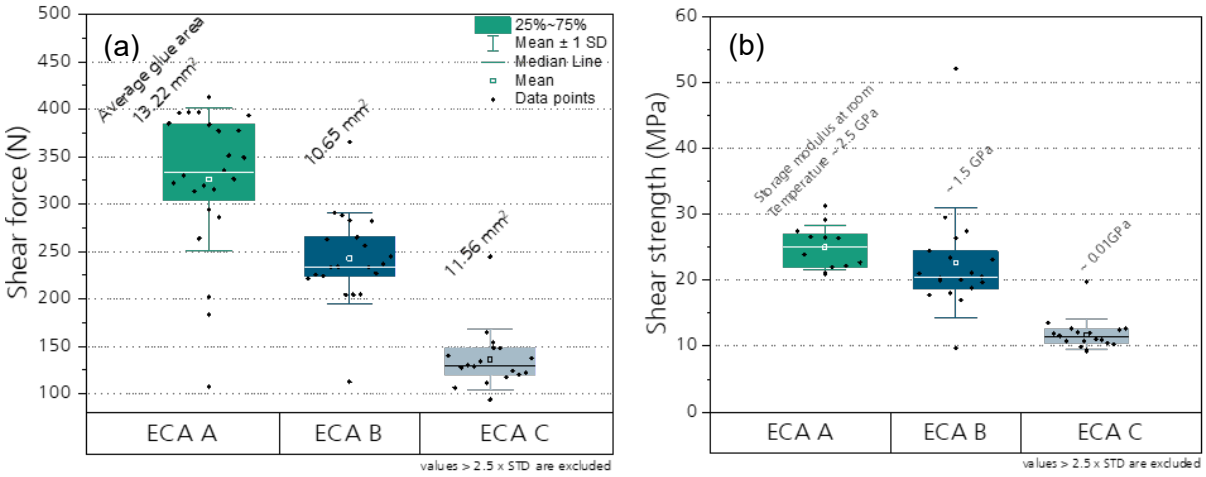

Figure 6. Box-Whisker plots of a) Die shear forces and b) Die shear strength of the three ECAs with the average glue area as well as storage modulus of each ECA

the bond between the metallization as in some samples the metallization was peeled off due to shearing. From the rest of the samples that did not have cell fracture as a failure mode (see Figure 7b), the ECA area was measured and the microstructure of the ECA after curing was investigated.

ECA B and C showed cohesive fracture close to the busbar in all sheared samples (Figure 7c, d). ECA B had the most noticeable number of voids with the biggest sizes in comparison to A and C. Existing voids, the general nonuniformity of the joints (although produced with automated methods) alongside the fact that the actual stress distribution in the joint is not uniform (according to finite element simulations not shown in this paper) were identified as reasons for the high tendency for outliers.

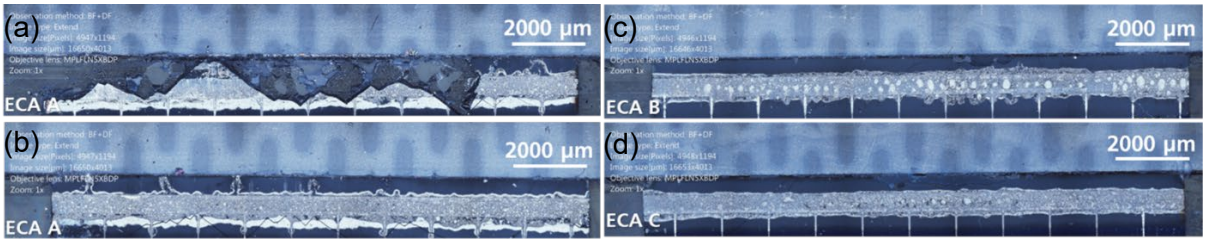

Figure 7. A top view of the front busbar a) after applying the die shear test on samples interconnected with ECA A. b) Example of cohesive shear of ECA A sample. c) Cohesive fracture around the busbar of ECA B where large voids can be seen. d) Cohesive fracture for ECA C.

As ECA B has the highest number of voids and the biggest void size, samples produced using ECA B were investigated more closely using SEM. From Figure 8, we see the high intensity of voids, that may be present already in the liquid ECA and form or extend during curing of the ECA. The void diameters range between 10 µm and 200 µm.

From Figure 8c, we see a tendency of the silver flakes to align perpendicular to the busbar around the walls of the void. In parts without voids the silver flakes tend to align in parallel to the busbar. Due to the perpendicular alignment of silver flakes an improvement in z-conductivity is expected in these areas. Although voids are usually considered undesirable in adhesive joints, here they could increase the electrical conductivity between the shingles.

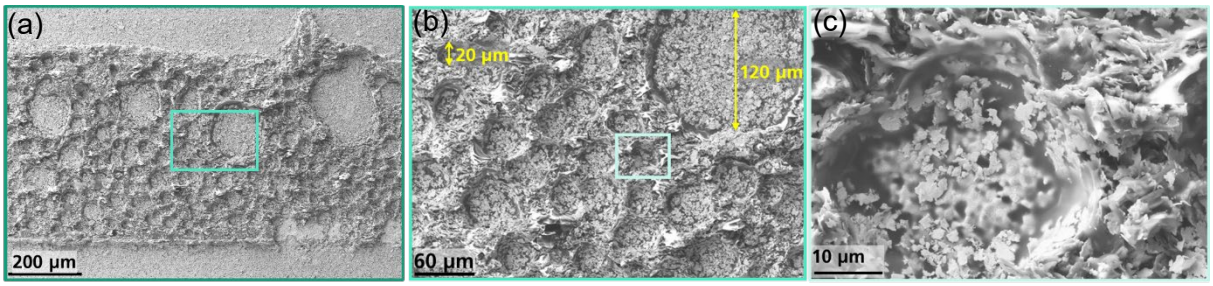

Figure 8. SEM view with three levels of magnification on a sheared sample of ECA B. a) Shows an overview of the sizes of voids the ECA. b) A closer look where big and small voids are seen in more details. c) The alignment of the conductive particles around a void's wall.

Finally, the full-size modules built from the three ECA were characterized using EL and *I–V* measurements at initial stage, after 200 thermal cycling and after mechanical load test with 5400 Pa (see Figure 9a in appendix). ECA A and B were not as much affected by degradation, although from EL images it was noticeable that the strings have cell cracks after ML5400Pa due to the limited flexibility of the two ECAs (Figure 9b in appendix). Although ECA C has less cell cracks, it showed subtle degradation (Figure 9b in appendix) of the electrical performance of the joint. This could be caused by a higher deflection of ECA C and plastic deformation due to mechanical stress. In this state the filler particles within the ECA may lose contact with each

other or to the busbar surface leading to local joint degradation. Table 1 shows the *I–V* characteristics of the modules before and after testing, where the I_{SC} and V_{OC} are mostly constant, and the degradation is shown by the *FF.* As can be seen, the cell cracks for modules with ECA A and B (Figure 9b in appendix) cause less power degradation than the overall joint degradation of many cells in the module with ECA C. Generally, the different failure modes, do not have a large effect on the performance of the modules indicating that the flexibility of the ECA in turn seems not to play such an important role as was expected. Thus, ECAs for shingle interconnection could be formulated in a wider range of flexibilities without compromising the mechanical stability in the final PV module. To support this outcome further tests should be applied on the produced modules to monitor the change in performance until all IEC tests have been passed.

Table 1. *I–V* characteristics of the full-size modules produced using the three tested ECAs, measured after production, after TC200 and after ML5400Pa

ECA	P_{MPP} (W)	Power loss (%)	V_{OC} (V)	I_{SC} (A)	*FF* (%)	State
A	323.6		43.1	9.7	77.5	**initial**
	323.6	- 0.0	43.1	9.7	77.7	**TC200**
	319.0	- 1.4	43.0	9.7	76.8	**ML**
B	322.5		43.0	9.7	77.4	**initial**
	321.6	- 0.3	43.0	9.7	77.3	**TC200**
	318.0	- 1.3	43.0	9.7	76.7	**ML**
C	325.0		43.1	9.7	77.7	**initial**
	322.0	- 0.8	43.1	9.7	77.3	**TC200**
	317.0	- 2.3	43.1	9.7	76.1	**ML**

4. Conclusions

The die shear test can be a useful method to determine the mechanical strength of shingle joints. The temperature variation as well as the amount of ECAs printed on the busbars affect the shear force and shear strength. A curing temperature of 110 °C led to lower shear strength of ECA D of (8.3 ± 2.8) MPa compared to (12.9 ± 1.9) MPa when cured at 150 °C. The width of the printed ECA correlated to the absolute shear force but had little effect on the strength.

The die shear test has a high tendency of outliers which is caused by nonuniformities such as voids that form during curing or are already present in the liquid ECA.

Three chemically similar ECAs with the same silver content were characterized by DMA. The T_g varies between 120 °C for ECA A, 90 °C for ECA B to 15 °C for ECA C along with the storage modulus at room temperature. The T_g and storage modulus at room temperature correlated to the shear strength and fracture pattern. ECA A, as the stiffest of the materials, had the highest shear strength of (24.9 ± 3.3) MPa and the highest possibility for substrate (cell) fracture during shear test. ECA B and ECA C tended to break cohesively and had a shear strength of (23.6 ± 9.2) MPa and (15.3 ± 8.5) MPa, respectively.

Full format shingle modules with all three ECAs had the same initial performance and, overall, had only a small degradation of maximum 2.3% after TC 200 and ML 5400 Pa. The ECAs with higher strength and lower flexibility showed slightly lower degradation than the flexible one with lowest strength.

Data availability statement

The data used in this study were accessed with permission from the authors. If data access for further use is needed, interested parties must contact the authors directly to request the data

Author contributions

Najwa Abdel Latif: Carried out the variation of mechanical properties of ECA experimental and data analysis parts, wrote the original draft, and performed the final edits.

Rachid Lamsairhri: Carried out the variation of ECA printing width and curing temperature experimental and data analysis parts.

Torsten Rößler: Carried out the dynamic mechanical data analysis, reviewed and provided feedback on the manuscript, as well as supervising the whole work scope.

Competing interests

The authors declare that they have no competing interests

Funding

The work in this paper was funded by the SHIRKAN project and supported by Federal Ministry for Economic Affairs and Energy on the basis of a decision by the German Bundestag.

Acknowledgement

We would like to thank Polytec PT for developing the Electrically Conductive Adhesives used in this work.

References

[1] Puzant Baliozian, Nils Klasen, Nico Wöhrle, Christoph Kutter, and Ralf Preu, PERC-based shingled solar cells and modules at Fraunhofer ISE - Photovoltaics International Vol 43 (43), 2019. [Online]. Available: https://www.researchgate.net/publication/335992713_PERC-based_shingled_solar_cells_and_modules_at_Fraunhofer_ISE_-_Photovoltaics_International_Vol_43. Accessed: Nov. 14, 2022.

[2] 2nd International Conference on Emerging Smart Materials in Applied Chemistry. (ESMAC-2021): ESMAC-2021. AIP Publishing, 2023. Accessed: Nov. 14, 2022.

[3] H. Wirth, M. Heinrich, M. Mittag, E. Fokuhl, N. Klasen, and A. Mondon, “Comparison of Layouts for Shingled Bifacial PV Modules in Terms of Power Output, Cell-to-Module Ratio and Bifaciality,” 2018. [Online]. Available: https://www.semanticscholar.org/paper/Comparison-of-Layouts-for-Shingled-Bifacial-PV-in-Wirth-Heinrich/69c813cc143e36c415c241d28f5987c305fb2023. Accessed: Nov. 14, 2022. doi: https://doi.org/10.4229/35THEUPVSEC20182018-5BO.9.3.

[4] G. Beaucarne, “Materials Challenge for Shingled Cells Interconnection,” Energy Procedia, vol. 98, pp. 115–124, 2016. doi: 10.1016/j.egypro.2016.10.087. [Online]. Available: https://www.sciencedirect.com/science/article/pii/S1876610216310487. Accessed: Nov. 14, 2022.

[5] N. Klasen, A. Mondon, A. Kraft, and U. Eitner, Shingled Cell Interconnection: A New Generation of Bifacial PV-Modules, 2018. doi: 10.2139/ssrn.3152478. [Online]. Available: https://papers.ssrn.com/sol3/papers.cfm?abstract_id=3152478. Accessed: Nov. 14, 2022.

[6] D. Tonini, G. Cellere, M. Bertazzo, A. Fecchio, L. Cerasti, and M. Galiazzo, “Shingling Technology For Cell Interconnection: Technological Aspects And Process Integration,” Energy Procedia, vol. 150, pp. 36–43, 2018. doi: 10.1016/j.egypro.2018.09.010. [Online]. Available: https://www.sciencedirect.com/science/article/pii/S1876610218305502. Accessed: Nov. 14, 2022.

[7] T. Rößler et al., “Progress in shingle interconnection based on electrically conductive adhesives at Fraunhofer ISE,” AIP Conference Proceedings, vol. 2709, no. 1, p. 20012, 2022. doi: 10.1063/5.0127455. [Online]. Available: https://pubs.aip.org/aip/acp/article/2709/1/020012/2832446/Progress-in-shingle-interconnection-based-on. Accessed: Nov. 14, 2022.

[8] Solarzellen - Datenblattangaben und Angaben zum Produkt für kristalline Silizium-Solarzellen, DIN EN 50461:2006, Deutsches Institut für Normung e.V., Berlin, Mar. 2007.

[9] DIN EN ISO 10365:2022-05, Klebstoffe_- Bezeichnung der wichtigsten Bruchbilder (ISO_10365:2022); Deutsche Fassung EN_ISO_10365:2022, DIN EN ISO 10365:2022-05, Deutsches Institut für Normung e.V., Berlin.

[10] Microcircuit test standards, MIL-STD-883F, Department of Defense, Method 2019.7, Die Shear Strength.

[11] A. Büchler, “Interface study on laser-structured plated contacts for silicon solar cells,” Dissertation. Albert-Ludwigs-Universitat Freiburg im Breisgau, 2019.doi: 10.6094/UNIFR/149376. [Online]. Available: https://freidok.uni-freiburg.de/data/149376. Accessed: Oct. 24, 2022.

[12] D. Tune, K. Wienands, I. Ullmann, M. Ignacia Devoto, T. Timofte, and A. Halm, “Electrically Conductive Adhesive Interconnects: How Low Can You Go?,” (4 pages / 38th European Photovoltaic Solar Energy Conference and Exhibition; 735-738), 2021, doi: 10.4229/EUPVSEC20212021-4AV.1.16. Accessed: Feb. 02, 2023.

[13] S. Hoffmann, T. Geipel, M. Meinert, and A. Kraft, “Analysis of Peel and Shear Forces after Temperature Cycle Tests for Electrical Conductive Adhesives,” (4 pages / 33rd European Photovoltaic Solar Energy Conference and Exhibition; 183-186), 2017, doi: 10.4229/EUPVSEC20172017-1CV.3.91. Accessed: Oct. 19, 2022.

[14] D. Kutzleben et al., “Development of shingle matrix technology for integrated PV applications,” doi: 10.4229/WCPEC-82022-3CO.4.4. Accessed: Feb. 21, 2023.

[15] D. Eberlein, P. Schmitt, and P. Voos, “Metallographische Probenpräparation von verlöteten Solarzellen,” Practical Metallography, vol. 48, no. 5, pp. 239–260, 2011, doi: 10.3139/147.110129. Accessed: Mar. 06, 2023.

[16] Practice for Plastics: Dynamic Mechanical Properties: Determination and Report of Procedures, ASTM D 4065:2020, D20 Committee, West Conshohocken, PA.

[17] M. Sepe, Dynamical Mechanical Analysis for Plastics Engineering. Plastics Design Library, 1988. Accessed: Apr. 28, 2023.

[18] Terrestrial photovoltaic (PV) modules – Design qualification and type approval – Part 2: Test procedures, IEC 61215-2, IEC, 01.03.202016.

Appendix

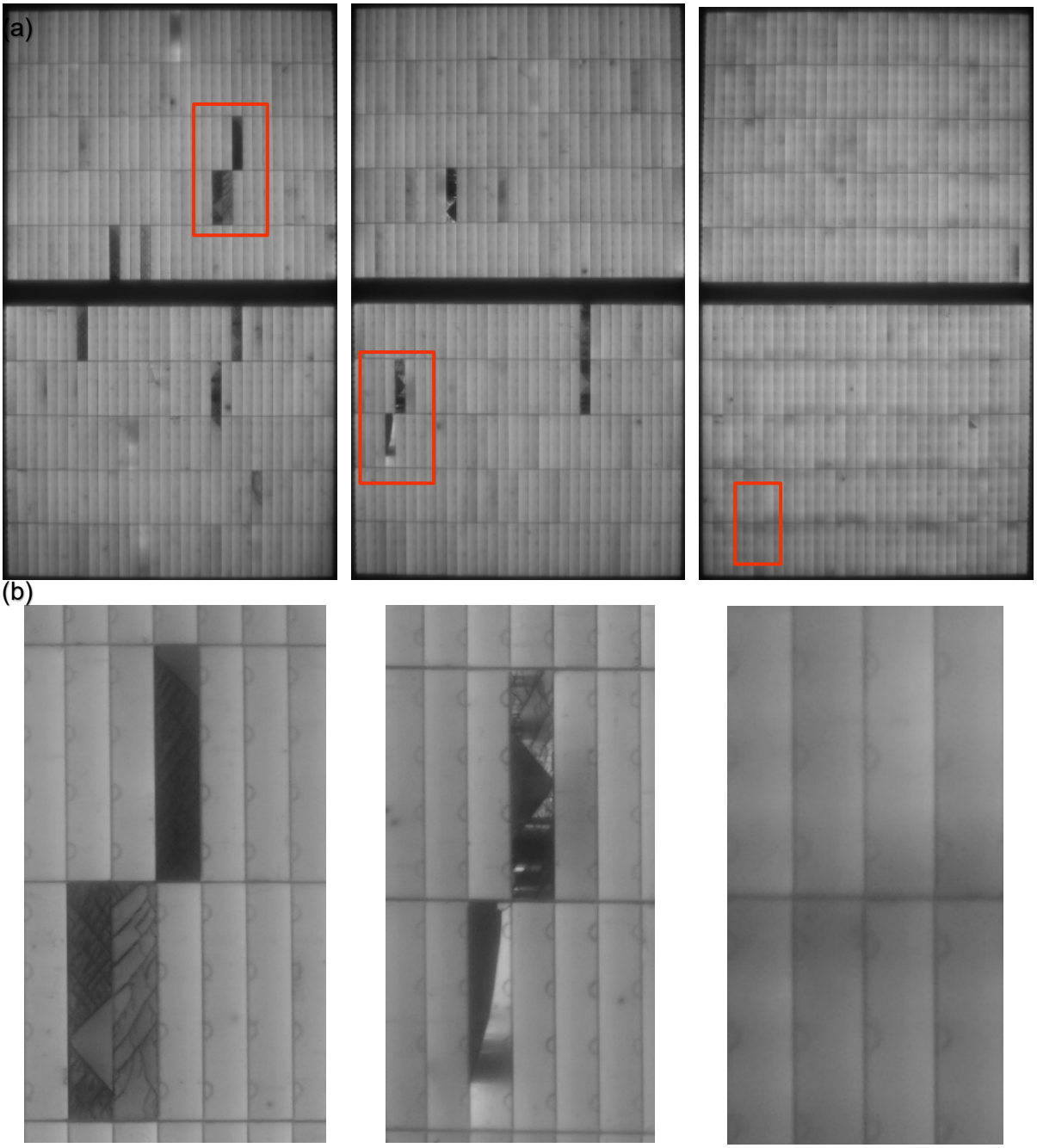

Figure 9. a) EL images of full-size modules after being subjected to TC200 and ML 5400Pa for modules produced from the three tested ECAs (A. B, and C respectively). b) a close up on the failure modes the different modules underwent after the last test (ML) where for ECA A and B we see cell fractures after applying the load, while C shows degradation of the interconnection between the shingles.